Magnetically levitated reaction wheel for space application

A. Argondizza, S. Carabelli, G. Genta, A. Tonoli

Mechatronics Laboratory – Centro Servizi di Prototipazione
Politecnico di Torino
Corso Duca degli Abruzzi, 24
I-10129 Torino, Italy

Summary

The content of the present study is the feasibility assessment of a reaction wheel on active magnetic bearings (AMB) to be followed by the design of a fully operational engineering model[1], which is presently under construction. The stress is laid mainly on the demonstration that a small, simple reaction wheel on AMB can be built and operated reliably with power requirements which are not in excess than those characteristic of conventional units.

A reaction wheel is usually a part of a complex system whose task is the attitude control of a spacecraft and in some cases also the storage of energy in the form of kinetic energy in the rotor. Here the work is concentrated only on the reaction wheel component, intended as a torque actuator. No attempt to address the problems related to the global system or to the possibility of using the reaction wheel as an energy storage device is performed.

AMB technology is at present a well known technology in high speed rotating machinery. Several prototypes of machines of various kinds in which the rotor is magnetically suspended have been built and in some cases are on the market. Several applications of reaction wheels have been studied and many reaction wheels operating on AMB have been built, starting from the seventies[2]. The present study is intended to address some specific problems, mostly related with low power consumption, high system integration and design compactness.

General architecture

The starting requirements were limited to those listed in table 1 in order to leave many open choices to the designer. In particular the maximum torque that the motor must supply to the wheel and the operational speed range have not been explicitly stated. The requirement on the maximum torque has no impact on the design of the wheel itself but is related to the power consumption, not only while producing torque but also while spinning in no torque conditions as the size of the motor influences the power losses in all conditions.

[1]The feasibilty study has been accomplished under contract 730-08-06527 from University of Houston (USA).

[2]A number of papers are available in the proceedings of the conferences on flywheel energy storage (San Francisco 1976, Scottsdale 1978), on active magnetic bearings (Zurich 88, Tokyo 90, Alexandria 92, Zurich 94, Kanazawa 96) and on magnetic suspension (sponsored by NASA). Other related papers were presented at the flywheel energy storage sessions of IECEC.

Angular momentum	≥ 3.5	kg m^2 s^{-1}
Wheel mass	≤ 1	kg
Wheel diameter	≤ 200	mm
Wheel thickness	≤ 60	mm
Five active axes magnetic suspension		
DC brushless motor		
Digital integrated AMB, controller and motor drive		

Table 1: General requirements given at the contract formalization.

Torque and power requirements together affect the choice of the working speed range. For the parameters not explicitly stated, a torque of 0.03 N m over a speed range of $\pm$10,000 rmp were assumed as design objectives.

Wheel configuration In order to obtain the required angular momentum at a fairly low speed, a pierced disc with rim and central hub configuration has been chosen. The higher stress level, if compared with other configurations, is of no concern here as the peripheral velocity is very low.

Active magnetic bearings In order to limit the axial thickness of the rotor, a conical configuration for the magnetic bearings has been chosen. The conical bearings allow radial and axial forces to be produced without the need for a separate axial bearing. Moreover, the conical bearings are "O" mounted to improve the bearings load capability in order to compensate for the gyroscopic torque.

To keep to a minimum the number of power drives, each AMB actuator includes three horseshoe shaped electromagnets. The resulting six magnetic forces are enough to constrain the five degrees of freedom of the rotor.

An optical solution for colocated displacement sensors is proposed. Its main advantages are: integration within the magnetic actuator, low sensitivity from electromagnetic interferences and simple signal electronics.

Motor In order to limit the axial thickness of the system, a DC brushless motor with external rotor has been devised. The rotating permanent magnets are actually installed in the flywheel hub. The internal stator with the motor windings is mounted on the central shaft. The motor is driven to provide a constant torque in either directions.

Electronic control unit In order to obtain an electronic control unit as integrated as possible, a number of highly integrated components has been chosen. The computing unit is a fixed point digital signal processor (DSP) with integrated PWM outputs, A/D and capture inputs. Moreover, the power electronics for AMB and motor drives have been chosen to be directly interfaced to the DSP outputs.

Housing and locking The wheel, the bearings and the motor are in vacuum, together with the sensors and the sensor electronics. The electronic control unit is in a separate housing, not vacuum tight, to be mounted either on the wheel housing or at a certain distance from the main unit.

Whenever the wheel is in non operating conditions, one of the conical bearing can be used together with the landing bearings to lock the wheel against high vibrations or accelerations.

Reaction wheel

A minimum value of speed and moment of inertia of the reaction wheel can be easily assessed:

$$J_{\max}\omega_{\max} \geq M_a \tag{1}$$

where $\omega_{\max}$ is the minimum value of the top speed, M_a is the stated angular momentum and $J_{\max}$ is the maximum moment of inertia compatible with the mass and the external envelope constraints. The shape which uses at best the allowed envelope is a circular hollow cylinder.

The higher the speed, the lighter the wheel can be. This consideration is limited by the allowable strength of the material (centrifugal stressing grows with the square of the peripheral speed) and by the maximum speed at which the chosen bearings can work. However, while this consideration is very important in the cases in which the angular velocity (or, better, the peripheral velocity) can be chosen without strict constraints and the limitations come only from the allowable strength of the material, as in the case of energy storage flywheels, in the present case the peripheral velocity is limited by the requirement of limiting the maximum power P needed to produce a given reaction torque T:

$$P = T\omega \tag{2}$$

As a trade-off between the mass of the wheel and the power of the motor generator, a value of 10,000 rpm is assumed for the maximum spin speed. The wheel must then have a moment of inertia

$$J = 0.00334 \text{ kg m}^2 \tag{3}$$

To exert the required torque of 0.03 Nm at 10,000 rpm, the motor must therefore supply a power

$$P = 31.4 \text{ W} \tag{4}$$

Rotor design

The ratio between the angular momentum $J\omega$ and the mass m of the rotor can be expressed as

$$\frac{J\omega}{m} = 2K\frac{\sigma_{\max}}{\rho\omega} \tag{5}$$

where K and $\sigma_{\max}$ are the shape factor, depending only on the geometry of the rotor, and the maximum stress present in the material. At equal speed ω, maximum strength and material density ρ, the shape which allows the maximum value of the ratio between the angular momentum and the mass is that which is characterized by the maximum value of the shape factor, namely the constant stress disc. The stressing of the flywheel can thus not be the limiting factor and a disc-with-rim rotor can have performances exceeding those of a constant stress disc.

In the present case, a shape which minimizes the mass for the chosen momentum J and for the given external envelope constraints has been selected. The values of the stresses will be shown to be fairly low and a shape which maximizes the radius of inertia can be used. A disc with rim configuration has then been chosen. A pierced disc configuration has the added advantage of allowing the location of the motor inside the wheel, reducing the axial length of the system.

To reduce the mass of the disc without resorting to a very thin wall and to reduce centrifugal stressing, a light alloy has been chosen for the wheel. The stub shafts are made in one piece with the wheel.

The total mass and the moment of inertia of the wheel are 0.459 kg and 0.00349 kg m^2. Slightly higher values are to be expected owing to the presence of fillets at the disc-rim interface. The hub, the bearings and the rotating parts of the motor further increase the rotor mass.

The inertia properties of the wheel assembly, including the rotating parts of the magnetic bearings and motor are reported in table 2.

Rotordynamic analysis

The rotordynamic analysis of the wheel is aimed to verify that no critical speed linked to the wheel deformation modes falls in the working range of the machine. A free-free finite element model of the wheel, with its integral shaft, the laminations of the magnetic bearings and the rotor of the electric motor has been built. As usual, the laminations of the bearings and the permanent magnets of the motor have been modelled as distributed inertias located on the stub shafts, which has been considered as the only element which provides stiffness.

To take into account possible deformation modes of the wheel disc, the wheel has been modelled using suitable deformable disc elements, which take into account both centrifugal stiffening and gyroscopic effects. The model includes 17 nodes, 9 Timoshenko beam elements, 7 disc elements and one shaft-disc transition element. The total number of complex degrees of freedom is 50, then reduced to 17 after performing Guyan reduction.

The first critical speed related to deformation modes is 98,500 rad/s = 941,000 rpm and the analysis of its mode shows that it is due to shear deformation of the stub shafts. It is definitely outside the working range. The first two natural frequencies of the free-free rotor (Figure 1) at standstill and at the maximum speed of 10,000 rpm are reported in table 3.

The modes corresponding to the lowest natural frequencies are related to bending deformations of the disc. The very strong gyroscopic effect is clear: the disc deformation modes do not yield any critical speed, as conical modes are very much affected by the speed. The first mode which is mainly a cylindrical one has a natural frequency which is very high.

The rotor works in the low subcritical range, with respect to deformation modes, and its dynamics is that of a rigid rotor with very high gyroscopic effect (high ratio between polar and transverse moments of inertia) supported on magnetic bearings.

Load conditions

No requirements regarding external loads or gyroscopic moments have been explicitly stated. The inertia wheel has to operate in a microgravity environment but the engineering model must be tested on the ground. It is therefore reasonable to require that the wheel is able to operate under a gravitational acceleration load of 1 g in all directions. This value of the load, augmented by a suitable safety factor, will be used in designing the bearings. This choice leads

Mass	0.796	kg
Polar moment of inertia	0.00364	kg m^2
Transversal moment of inertia	0.00188	kg m^2

Table 2: Reaction wheel: inertial properties.

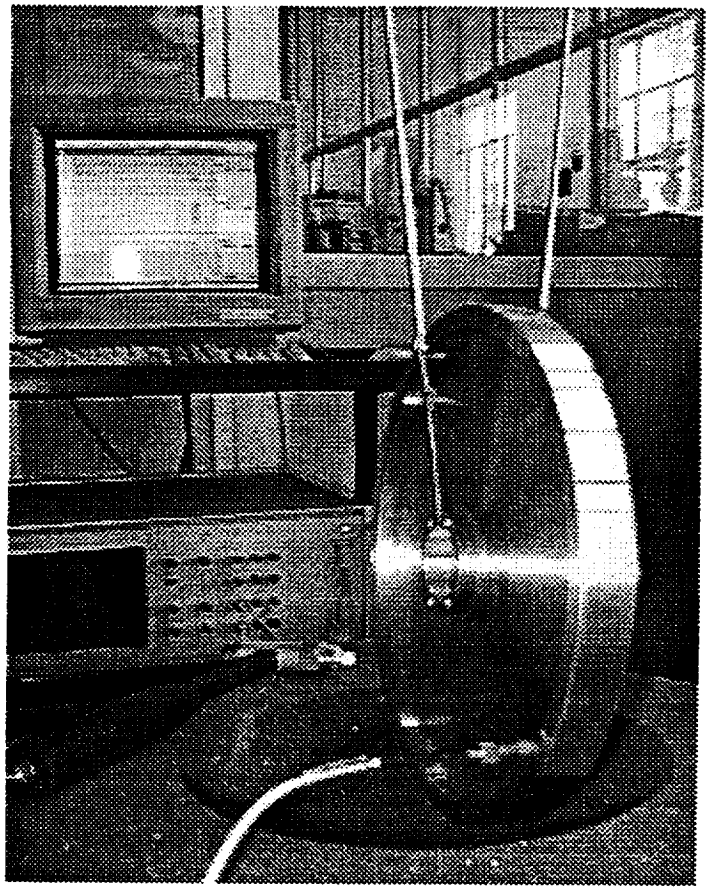

Figure 1: Free-free test for the validation of the FE model of the wheel.

to an overdesign of both the electromechanical parts and the power electronics relative to the microgravity operating conditions. However this has little effect on the power consumption and the mass of the systems and has two advantages: the bearings operate with very low magnetic induction, and hence with very low eddy current drag. In addition, severe requirements regarding acceleration and gyroscopic moments can be met by the engineering model. The no-torque power consumption while operating in 1 g environment will be greater than that which will occur in actual microgravity operation.

Mode	at standstill		at 10,000 rpm	
	[rad/s]	[Hz]	[rad/s]	[Hz]
1st Forward	3130	498	4120	656
1st Backward	3130	498	2780	443
2nd Forward	16330	2599	17960	2859
2nd Backward	16330	2599	15920	2534

Table 3: Free-free rotor: first two deformable body natural frequencies.

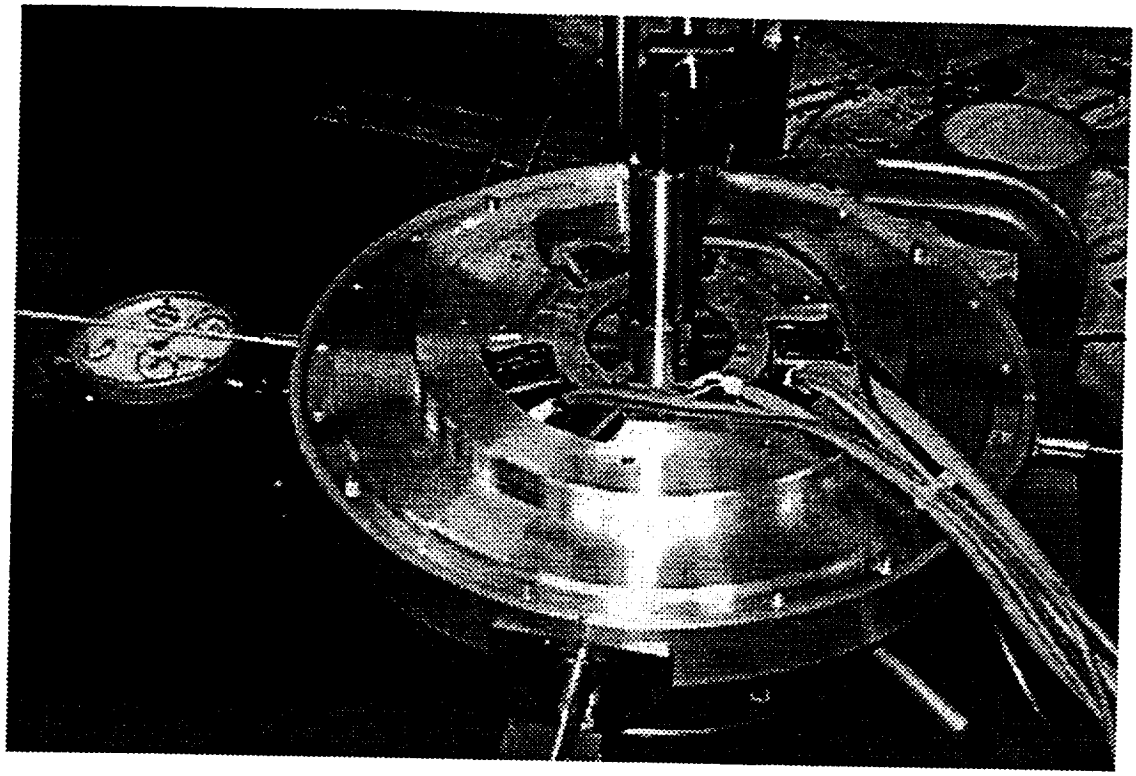

Figure 2: Reaction wheel under radial force tests.

Stator design

The main housing must contain the wheel in a vacuum environment. To allow an easy mounting and registration of all the internal components, the design includes two separate halves, which carry the bearing magnetic circuits and coils, the sensors and related local electronics, and two covers which, at the center, are connected by a central and nonrotating shaft, carrying the motor stator.

The electronic control unit is located in a separate housing, not vacuum tight. It is axially attached to the main one and cylindrically shaped to fit the wheel housing. Alternatively, it can be located at a certain distance from the main unit.

A vacuum connection will be located on the housing for evacuating the housing during laboratory tests. The simplest location for a vacuum flange is at the center of the left cover: the air can be pumped out through the central hollow shaft and the holes in the covers used to pass the cables.

Active magnetic bearings

In order to operate the active magnetic bearings, several **subsystems** must be properly designed and integrated: the AMB electromechanics made by the magnetic circuits and the coils, the rotor displacement sensors, the power electronics to drive the electromagnets, and the stabilizing controllers.

In non conical AMB configurations, each mechanical degree of freedom can be separately actuated, sensed and, most of the times, controlled. The AMB configuration here adopted

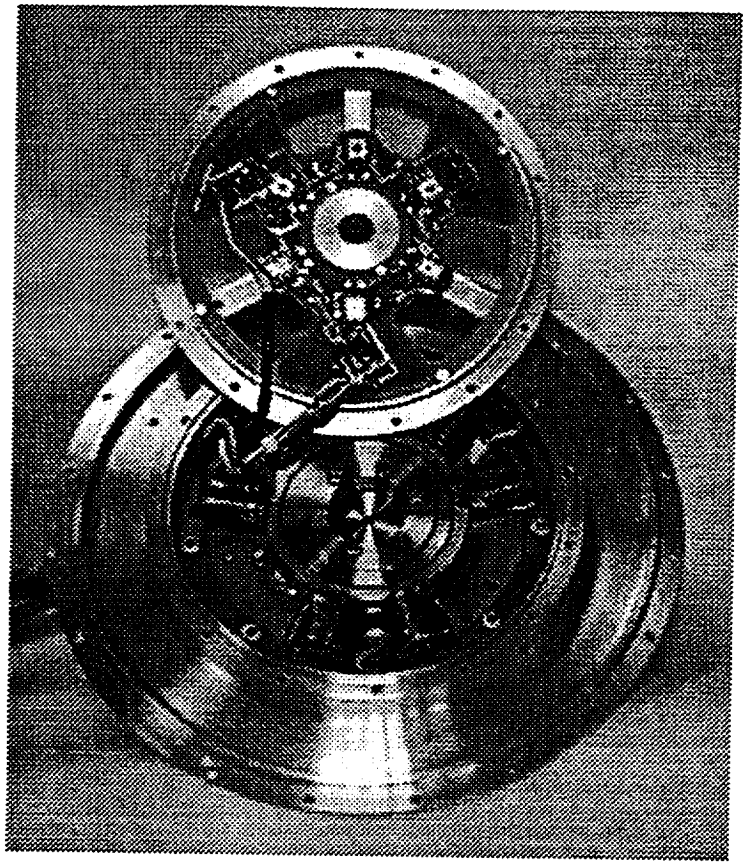

Figure 3: Reaction wheel in exploded view of optical sensors and electromagnets.

(Figure 3) includes two conical bearings with three electromagnets each to control the five degrees of freedom of the rotor. It should be noted that this layout intrinsically couples the radial and axial behaviors: each electromagnet produces a radial as well as an axial force at the same time.

The analog to digital converters integrated in the DSP (see 6) allows the sampling of two signals at a time. This is compatible with both the aforementioned sensor configurations in terms of computation efficiency, but only in the case of decentralized control.

Optical displacement sensors

Optical displacement sensors based on the measure of the light flux passing through the gap between the stator and the rotor are here used to measure the rotor to stator relative displacements. The light flux is related to the amplitude of the gap, its measure allows therefore to determine the relative position of the rotor. Each sensor is made of a light source, namely a light emitting diode (LED) and a light measuring device, namely a photodiode (for example Burr Brown OPT210P [1]). They are installed on opposite sides of each electromagnet so that the light emitted by the LED passes through the gap and illuminates the corresponding photodiode.

Six displacement sensors are installed on each AMB with a 60° angular spacing. Their angular location is the same where the forces produced by the three magnetic actuators are acting.

This setup has been chosen for the following reasons:

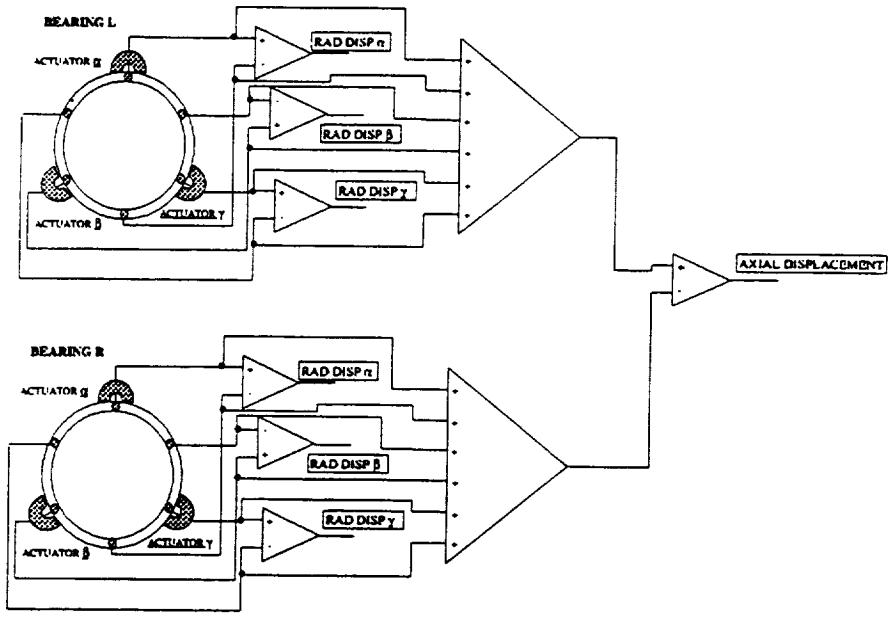

Figure 4: Block diagram of the signal electronics for the optical displacement sensor.

- redundancy: in the case a single sensor fails, the sensor located at 180° can be used instead of it with minimum system reconfiguration;
- flexibility: several connection schemes between the single sensors are possible with this configuration, this allows the adoption of different controller architectures;
- colocation: the sensors allow to measure the displacements along the directions where the AMB forces act.

A possible connecting configuration is shown in figure 4. The differential connection of the sensors at 180° is used to obtain a measure of the displacement along the diameter connecting the two sensors. This measure is decoupled from the axial displacements and from the displacements in a direction perpendicular to the diameter. The summing connection of the same sensors is used to obtain a measure of the axial displacements which is decoupled from the radial displacements.

The optical sensors used here are intrinsically colocated with the actuators, i.e. each of them measures the displacement in the same direction of the force produced by the corresponding electromagnet. In their simplest configuration, they can be directly used to implement a fully decentralized control, i.e. each measurement is fed back to a separate control that computes the driving command to be applied to the corresponding (colocated) actuator.

Electromagnets

Under the assumptions of

- no magnetic saturation in the iron core and
- no flux leakage out of the magnetic circuit in the air gap,

Maximum force ($\sim$ 2 g)	19	N
Maximum current	3	A
Pole cross section at the air gap	60	mm^2
Nominal air gap t_0	0.3	mm
Number of turns	95	
Coil resistance	0.19	Ω
Maximum field in iron	0.85	T
Bias current i_0	0.1	A
Nominal current density	0.2	A mm^{-2}
Nominal dissipated power	19	mW
Coil inductance L	1.1	mH
Force/current factor $= L\frac{i_0}{t_0}$	0.38	N A^{-1}
Force/displacement factor $= L\left(\frac{i_0}{t_0}\right)^2$	127	N m^{-1}

Table 4: Active magnetic bearing: main characteristics.

the force F_m generated by each electromagnet depends only on the induced magnetic field B and on the magnetic circuit cross section in air S_{air}

$$F_m = \frac{S_{air}B^2}{\mu_0} \tag{6}$$

where μ_0 is the magnetic permeability. The iron cross section along the magnetic circuit is relevant only as far as it does not induce saturation of the induced magnetic field. In order to avoid saturation, a geometrical relation of 1:1 is usually applied for the iron pole width and lamination radial width with respect to the pole width at the air gap. In case a lower ratio is needed for design reasons, a local check of the magnetic field must be carried out. The saturation limit is here assumed conservatively to 1 T.

The radial dimensions of the bearing slot depends on the characteristic of the coils it is supposed to house. A compromise must be found between the copper (or aluminum) wire section in order to have low thermal dissipation and the overall weight of copper and iron parts. Under steady state operation, a bias current of 100 mA is here supposed for each coil with a relatively low current density of around 0.2 A/mm^2 for a total heat dissipation of 20 mW for each coil. This value must be kept low because the dissipation is possible only by radiation since the bearing stator is under vacuum.

The main parameters of the designed electromagnets are summarized in table 4.

Control

The general scheme for the electromagnet control subsystem is sketched in figure 5. The presence of two analog to digital converters allows to sample simultaneously the current and the position signals for each electromagnet. With a decentralized control algorithm, it is possible to compute the command to set the PWM output while waiting for the conversion of the sampled current and position signals for the next multiplexed electromagnet.

The differential configuration of the optical sensors provides 6 decoupled purely radial displacement measurements and 1 purely axial displacement measurements. This set of measurements is intrinsically redundant to control the five degrees of freedom that fully characterize the rotor behavior.

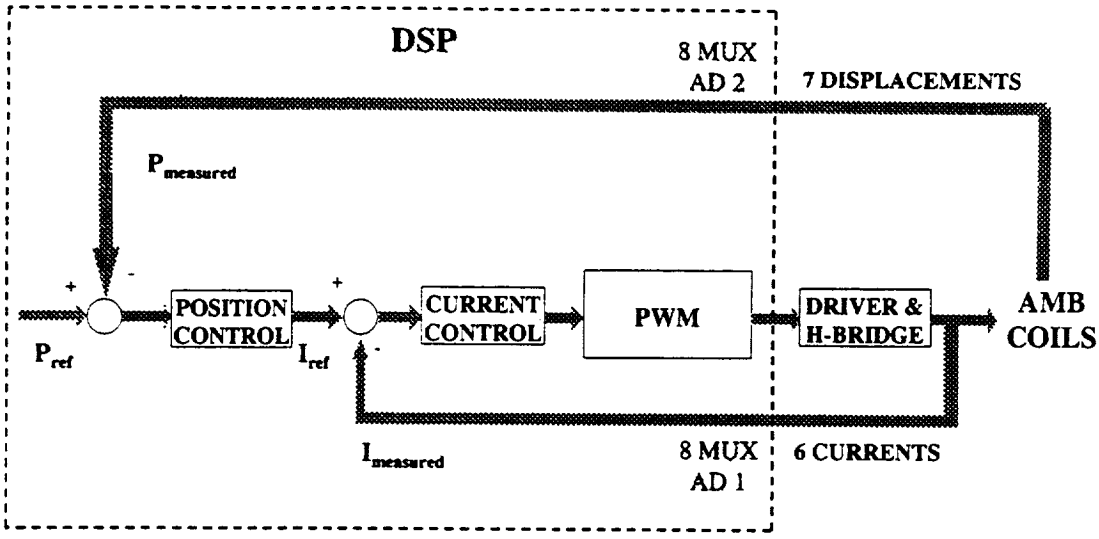

Figure 5: Block diagram for the electromagnet control subsystem.

It should be noted that, if a centralized control is adopted, every control output is setting a value to all the PWM outputs to the coils. A radial command usually drives three different coils to obtain a bidirectional force. In addition because of the conical shape of the bearing, any radial command also produces an axial action that can be compensated by equally actuating the three electromagnets on the opposite bearing. Actually, the PWM settings are updated after the computation of each control but the PWM commands are sent to the drivers of the power amplifier bridge only at the end of every sampling period.

Electronic control unit

The electronic control unit (ECU) is based on a digital signal processor (DSP), that manages all the system operations. The ECU also includes the external memories, the programmable logic and the AMB and motor power drives (figure 6).

The DSP choice strongly influences the overall machine layout: actually the use of the TMS320F240 DSP [2], that provides on a single chip the A/D converters, the PWM generation, the capture inputs, along with the timers and the computing unit, yields to a very compact ECU design, with a minimum amount of external components. Moreover, in the power electronics components selection, attention was paid to find integrated devices so as to reduce the total component number.

The system must be able to operate as a stand-alone machine and to be connected to a local and/or a remote interface. At power up the DSP is reset and the execution starts from the on-chip flash memory, programmed to load the code from the external **nonvolatile** RAM (NVRAM) into the external fast static RAM (SRAM). Once the code is loaded into the SRAM, the program execution starts. A programmable logic device (PLD) is responsible for the address decoding, the wait state generation to access the slow NVRAM and the reset logic.

To accomplish the need for an external interface, without DSP overloading, a dual port RAM (DPRAM) has been chosen. This allows to easily give accessibility to the relevant control and system parameters and variables, both for monitoring and tuning on-the-fly. If a dedicated bus

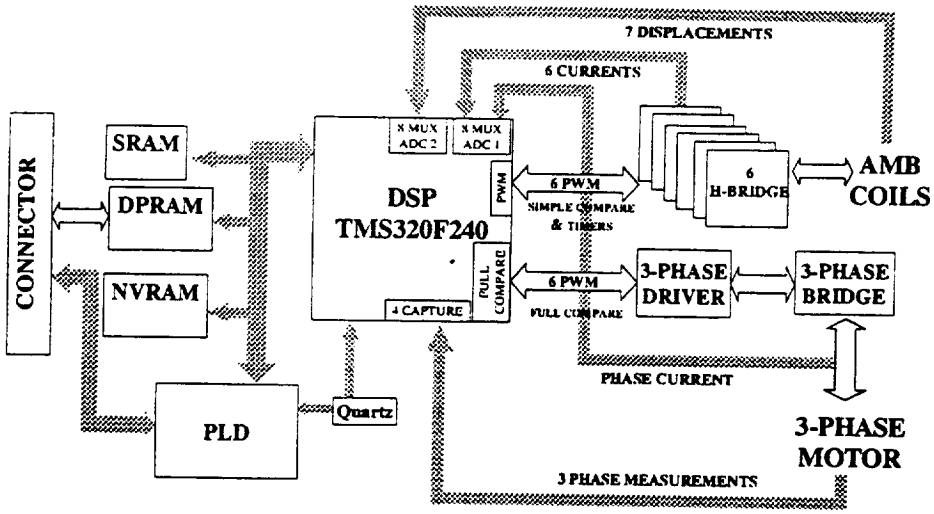

Figure 6: Electronic control unit functional block scheme.

is selected to interface the system to a host, then a PLD is needed to handle the interface. A single or two separate PLDs can be used to perform the ECU strictly necessary tasks and the bus interfacing: in the former case a larger device is necessary, but some redundancy is avoided, in the latter case a more compact solution for the ECU can be achieved.

The power to the AMB coils can be supplied by either linear or switching amplifiers: in the present case, to reduce the power consumption, the latter drives are selected. The DSP is able to directly provide the PWM signals necessary to drive the power stage that supplies the coil with the control current. An integrated H-bridge (including an internal current sense) has been found suitable for the AMB control [3] and has been tested at very low voltage supply (less than 15 V).

The brushless DC motor windings must be supplied by a 3-phase driver. An integrated device, suitable for the present application, is an SGS-Thomson 3-phase motor driver [4], with a high current capability (4 A) and a large supply voltage range; assuming a supply voltage of 15 V it can supply the motor with the requested power. Its inputs are directly connected to the DSP PWM outputs.

Conclusions

The present feasibility study shows the design configuration of a small, lightweight, highly integrated, low consumption reaction wheel based on the active electromagnetic bearing technology. The characteristics of the inertia wheel are summarized in table 5.

The main characteristics of the design are the following. It uses conical active bearings with the minimum number of coils, obtaining a five active-axis suspension with just six coils instead of the usual ten. The configuration used allows to positively lock the wheel against vibration and high accelerations when not rotating without resorting to a separate grabber system. Optical differential sensors are used instead of the more common eddy current or inductive sensors, with

System	Angular momentum	3.81	kg m^2s^{-1}
	Torque	0.03	N m
	Speed range	±10,000	rpm
	Diameter	220	mm
	Length (including ECU)	78	mm
	Length (ECU not included)	67	mm
Reaction wheel	Mass	0.796	kg
	Moment of inertia	0.00364	kg m^2
	Diameter	100	mm
	Thickness (at the hub)	36	mm
	Material	Light alloy (2014)	
Motor	Poles	6	
	Slots	9	
	Phases	3	
AMB	Bearings	2	
	Electromagnets	6	
	Maximum radial load	19	N
	Maximum axial load	15	N
Power consumption	Full torque	~ 40	W
	No torque	~ 6	W

Table 5: Reaction wheel: main characteristics.

notable advantages for what the actuator-sensor colocation, the electrical disturbance rejection and the overall cost is concerned. State-of-the-art digital electronics and purposely developed circuitry and software are used.

The whole system is very compact, with some of the electronics located within the wheel housing and the ECU with the power electronics located in a separate housing, axially to the wheel. All the subsystems are designed with ample margins, allowing the possibility of upgrading the performance, particularly where the maximum angular momentum and maximum torque is concerned. The detailed analysis of all components will lead to reductions in mass.

The so-called engineering model is currently under construction and will be ready for testing in the first part of next year.

References

[1] "OPT210 Monolithic Photodiode and Amplifier 300 kHz Bandwidth at Rf = 1 MΩ - Data Sheet." Burr-Brown, December 1995.

[2] "TMS320C240, TMS320F240 DSP Controllers - Data Sheet." Texas Instruments, December 1997.

[3] "LMD18200 3A, 55V H-Bridge - Data Sheet." National Semiconductor, September 1996.

[4] "L6234 Three Phase Motor Driver - Data Sheet." SGS-Thomson Microelectronics, March 1998.

Appendix: Drawing and main parts

The basic layout drawing of the system is reported in figure 7 . The main parts are identified and labelled; other parts as screws, seals, etc. are just indicated or omitted. With reference to the included layout, the main parts are as follows:

1. Wheel. Material: aluminum alloy, tentatively 2014. Owing to the low stress levels, the exact material choice is not critical. A constant thickness disc with rim and central hub configuration has been chosen. The stub, hollow shaft is integral with the wheel.
2. Left housing. Material: aluminum alloy, tentatively 2014. Main part of the housing, carrying the left magnetic bearing. The housing protrudes inwards to carry the circuit board with the LEDs of the position sensors.
3. Left cover. Material: aluminum alloy, tentatively 2014. Housing cover, carrying the central non-rotating shaft (part 9) and the motor.
4. Left magnetic bearing electronics. Two printed circuit boards, containing the main left bearing sensor components and the relevant electronics. The cables to this board run in the hollow shaft (part 9) and through a hole in left cover (part 3).
5. Left magnetic bearing stator. It is made of 3 horseshoe electromagnets. The magnetic circuit is laminated. The cables to the coils run in the hollow shaft (part 9) and through a hole in (part 3).
6. Left magnetic bearing rotor. It includes the laminated magnetic circuit, plus the inner flange. The flange is of steel, but aluminum can be used to save weight.
7. Left landing bearing support. Material: steel. The support acts also as outer flange for the bearing rotor.
8. Sleeve. Material: aluminum alloy. It carries the left landing bearing and keeps in position the motor windings.
9. Central shaft. Material: steel. It is attached to the right housing cover (part 11), and is restrained from rotating by a pin set into the left housing cover (part 3). The cables to the left bearing and the motor run through the shaft.
10. Left landing bearing. Standard deep grove ball bearing with O.D. 24 mm, I.D. 15 mm, thickness 5 mm.
11. Right housing. Material: aluminum alloy, tentatively 2014.
12. Right cover. Material: aluminum alloy, tentatively 2014. Similar to part 3, left cover, except for the fact that it carries the vacuum tight connector for all cables connecting the motor and the magnetic bearings.
13. Right magnetic bearing stator. Same as the left one (part 5).
14. Right magnetic bearing electronics. Same as the left one (part 4), but the cables are directly attached to the connector on part 12.
15. Right magnetic bearing rotor. Same as the left one (part 6).
16. Motor permanent magnet. Cylindrical permanent magnet with six poles.
17. Right landing bearing. Same as the left one (part 10).
18. Washer. Material: aluminum alloy.
19. Motor laminations. The magnetic circuit with 9 slots is laminated. The cables to the coils run in the hollow shaft (part 9) and through a hole in the right cover (part 12).
20. Right landing bearing support. Same as the left one (part 7), but with the provision for allowing a larger displacement of the wheel to the left (locked wheel conditions).
21. Nut. To lock the central shaft to the right cover.
22. Electronic control unit housing. Material: aluminum alloy. It is not vacuum tight.

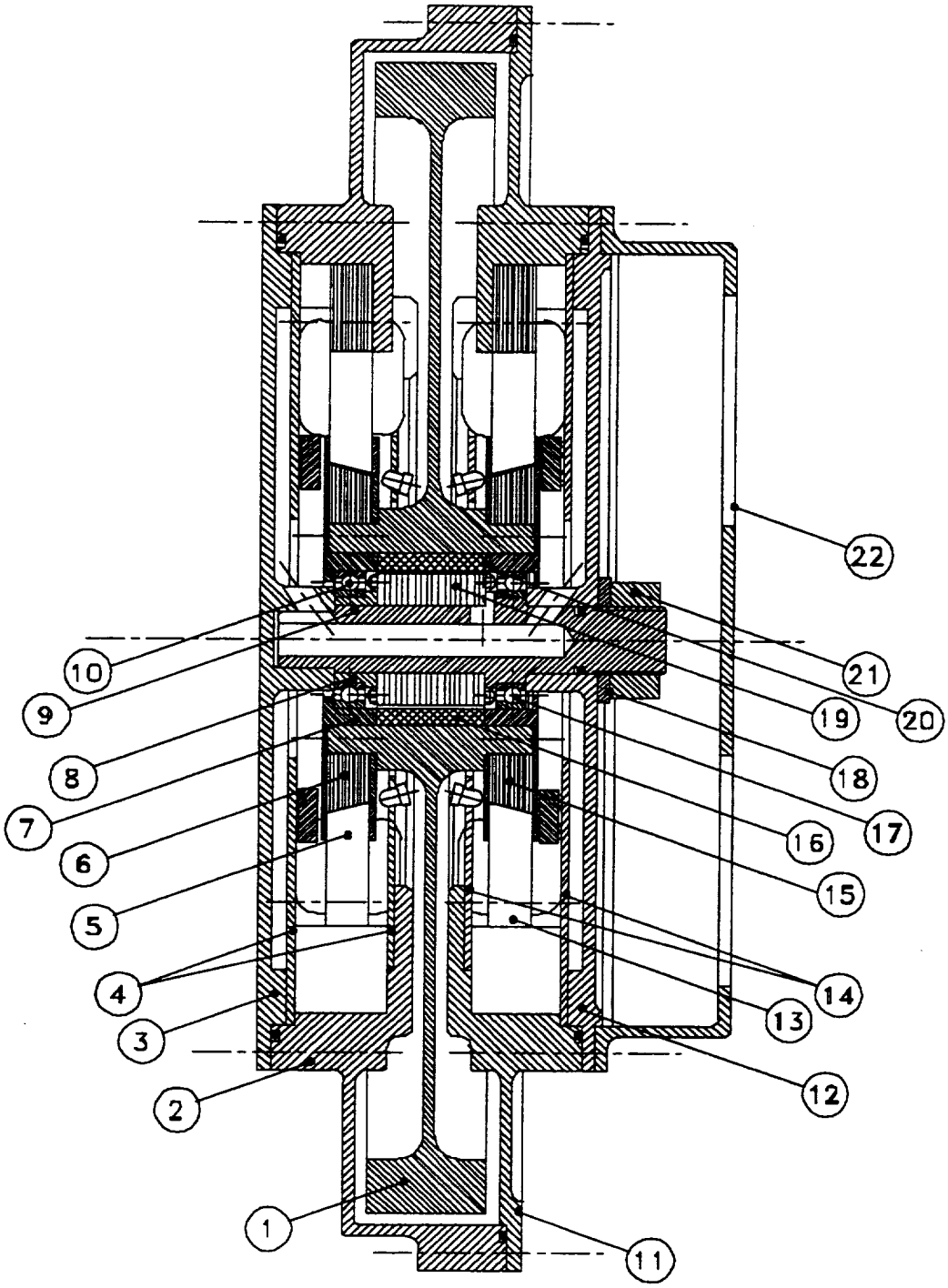

Figure 7: Reaction wheel section drawing (not to scale) with part numbers.